# Ion distribution models for defect fluorite $ZrO_2 – AO_{1.5}$ (A = *Ln*, Y) solid solutions: II. Thermodynamics of mixing and ordering

V.L. Vinograd[a,b†], A.A. Bukaemskiy[a]

[a] *Institute of Energy and Climate Research (IEK-6), Nuclear Waste Management and Reactor Safety, Forschungszentrum Jülich, Jülich, Germany.*

[b] *JARA High Performance Computing, Schinkelstrasse 2, 52062 Aachen, Germany*

Received; accepted

**Abstract**

Thermodynamic mixing properties of $A_xB_{1-x}O_{2-0.5x}V_{0.5x}$, fluorite-type solid solutions (B = Zr, A = {Nd-Yb, Y}, V = oxygen vacancy) are modelled as functions of four parameters, $\Delta H_1$, $\Delta H_2$, $\Delta H_3$ and $\Delta H_4$, which correspond to the enthalpy effects of the reactions $^6A + {}^8B = {}^7A + {}^7B$ (1), $^6A + {}^8B = {}^8A + {}^6B$ (2), $^6B + {}^8B = {}^7B + {}^7B$ (3) and $^6A + {}^8A = {}^7A + {}^7A$ (4), involving six cation species, $^6A$, $^7A$, $^8A$, $^6B$, $^7B$ and $^8B$. The model predicts that the disordered configuration containing all cation species evolves with the decreasing temperature such that 6-fold coordinated cations tend to vanish within $0 \le x \le 1/2$ domain, while 8-fold coordinated cations become extinct within $1/2 \le x \le 1$ domain. The further evolution within the intervals of $0 \le x \le 1/3$, $1/3 \le x \le 1/2$, $1/2 \le x \le 2/3$ and $2/3 \le x \le 1$ favours the extinction of $^7A$, $^8B$, $^7B$ and $^6A$ cation species, respectively. With the further decrease in the temperature 6-fold B and 8-fold A cations reappear within the domains of $1/3 \le x \le 1/2$ and $1/2 \le x \le 2/3$ via the reaction $^7A + {}^7B = {}^8A + {}^6B$. The configurational entropy reduces along with these transformations. The model fits structural and calorimetric data on Zr-based $A_xB_{1-x}O_{2-0.5x}V_{0.5x}$ systems and provides hints to understanding of ionic conductivity and radiation susceptibility data.

*Keywords: Defect fluorite, pyrochlore, thermodynamics of mixing, structure-property relationship, short range order*

## 1. Introduction

Order/disorder effects play a very important role in determining structure/property relationship of zirconia based yttria and lanthanide doped fluorite- and pyrochlore-type ceramics. Particularly, the ionic conductivity [1,2] and the radiation resistance [3-5] of pyrochlore-type $A_2Zr_2O_7$ compounds correlate with the propensity of these materials to undergo order/disorder pyrochlore/fluorite phase transformation [6,7]. In Part I [8] experimental data on nonstoichiometric $A_xZr_{1-x}O_{2-0.5x}$ systems systems, A = {*Ln*, Y}, were reviewed emphasising wending points in the structure/property relationships occurring at $x \sim 1/3$ and $x \sim$

1/2. The breaks in the structure/property dependencies were attributed to changes in schemes of short- and long-range order. Following previous theoretical studies [9-12] a proposition was made [8] that short-range order in Zr-based defect fluorite reveals itself in two main aspects, first, as the electrostatically driven avoidance of vacancies and, second, as the strain driven tendency of association of vacancies to cations of the smaller size. As shown in Part I [8], strict following these two tendencies gives rise to six models of SRO. The three models relevant for the domain of $0 \leq x \leq 0.5$, namely, DF1 ($0 \leq x \leq 1/3$), DF2 ($1/3 \leq x \leq 1/2$) and PY ($1/3 \leq x \leq 1/2$) were used to fit available *a* vs. *x* data, allowing for a successful description of vending points at $x \sim 1/3$ and $x \sim 1/2$.

The successful fit to *a* vs. *x* data with models of SRO gives an additional indication to the importance of SRO for the understanding of structure/property and phase stability relations in fluorite-type ceramics. This points out to the necessity of developing of a thermodynamic description of phase transformations in defect fluorite solid solutions, which includes the concept of SRO. Although the temperature of the pyrochlore/fluorite transition can be accurately estimated with a model that ignores SRO [13], there is an indication that the successful prediction of the transition temperature is a consequence of cancellation of errors in enthalpy and entropy terms. Indeed, in the study of Jiang et al. [13] the temperatures were calculated by combining differences in total energies between quasi-random structures of defect fluorite and ordered pyrochlore with the ideal configurational entropy of disorder in an $A_2B_2O_7$ compound. Notably, the latter differences exceeded the experimentally measured [14, 15] enthalpies of disorder in $Gd_2Hf_2O_7$ and $Eu_2Zr_2O_7$ in 2-3 times, suggesting that the ideal mixing model exaggerates the real entropy effect to the similar extent, and that the associated effects of SRO on the thermodynamic functions are huge.

Indeed, the large reduction in the entropy effect could be understood only under the assumption of a significant SRO remaining in defect fluorite above the transition temperature. A number of recent studies considered a weberite-type model of defect fluorite [11, 16, 17]. It was shown that the weberite model gives a good fit to pair distribution functions computed from total neutron scattering data on several defect

fluorite compounds [16]. Weberite is a polymorph of $A_2B_2O_7$, which can be derived from defect fluorite by ordering of vacancies and by allowing the mixing between A and B cations to occur only over a half of the total cation sites. Consequently, the configurational entropy of the weberite model is much smaller than this of a perfectly disordered defect fluorite. A series of quasi-random weberite structures with $A_xB_{1-x}O_{2-0.5x}$ composition were developed to model the effects of non-stoichiometry on the pyrochlore/fluorite transition in $ZrO_2$ - $NdO_{1.5}$ system [18]. The same study [18] noted, however, that the configurational entropy of weberite, particularly at the composition of stoichiometric pyrochlore, is too small to fit the measured enthalpy effect of disorder [15] in $Eu_2Zr_2O_7$, implying that defect fluorite should include more disorder than this allowed by the weberite structure.

In Part I [8] we developed phenomenological models of defect fluorite solid solutions which assumed different types of SRO to be stable in different composition domains. The models were shown to be consistent with *a* vs. *x* data on a number of $A_xZr_{1-x}O_{2-0.5x}$ systems, however, the role of these models within a temperature-dependent hierarchy of ordering states has not been investigated in detail. The aim of the present study is to add the temperature into the play. This is achieved via the development of a general statistical-thermodynamic model in which different types of SRO occur as consequences of the free energy minimization. While developing the general model the models DF1, DF2 and PY [8] ($0 \leq x \leq 0.5$), as well as their mirror models DF1M, DF2M and PYM ($0.5 \leq x \leq 1$), are re-derived here again starting from less ordered states. The set of models considered here is larger due to the need of describing increasing disorder at higher temperatures.

The model is composed of enthalpy and entropy terms. The total configurational entropy is combined of several limiting models between which gradual transitions are set with the aid of variational parameters. The enthalpy of mixing is set proportional to progresses of reactions between cation species through which mixed (ordered and disordered) states develop from the state of a mechanical mixture of the end-members $BO_2$ and $AO_{1.5}$. The entropy and enthalpy equations are combined to get a non-equilibrium Gibbs free energy equation, which is minimized at a given temperature with respect to the variational parameters.

The study provides a consistent justification of the models introduced in [8], revealing a more detailed relationship between SRO types occurring in specific temperature and composition intervals.

## 2. Models and Methods

### *2.1. Enthalpy of mixing*

In Part I [8] wending points in structure/property relations were linked to changes in SRO/LRO schemes and, ultimately, to changes in cation coordination numbers. Here we show that changes in thermodynamic properties can be also correlated with changes in coordination numbers of cations. Assuming that both endmembers $BO_2$ and $AO_{1.5}$ are built of $^{8}$B and $^{6}$A, respectively, and that the spectrum of coordination numbers is limited to the set {6, 7, 8}, the enthalpy of mixing can be primarily attributed to the enthalpy effects, $\Delta H_1$ and $\Delta H_2$, of the reactions

$$^{6}A + {}^{8}B = {}^{7}A + {}^{7}B, \quad (1)$$

$$^{6}A + {}^{8}B = {}^{8}A + {}^{6}B. \quad (2)$$

The reaction (2) stabilizes pyrochlore relative to the endmembers. The reaction (1) stabilizes a short-range ordered structure composed of 7-fold coordinated cations, which in Part I [8] was introduced as Stoichiometric Fluorite, the endmember of DF2 and DF2M models. The following reverse disproportionation reactions are also thought to occur within the solid solution affecting its enthalpy

$$^{8}B + {}^{6}B = {}^{7}B + {}^{7}B, \quad (3)$$

$$^{8}A + {}^{6}A = {}^{7}A + {}^{7}A. \quad (4)$$

The reaction (3) is expected to have a negative enthalpy effect for $ZrO_2$ as the coordination of 7 is consistent with the structure of the ground state baddeleyite. The enthalpy change due to reaction (4) is

more difficult to guess, as it apparently varies with the type (size) of A cation. However, one notes that the reactions (1), (2), (3) and (4) are not independent being linked through the following relationship

$$\Delta H_3 + \Delta H_4 = 2\Delta H_1 - \Delta H_2. \quad (5)$$

The latter relationship conveniently determines the sign and value of the enthalpy effect of reaction (4), when the values of the other terms are defined. As the cation species featuring at the right sides of these reactions occur only due to the solid solution formation, being absent in the endmembers, the enthalpy of mixing relative to the endmembers $BO_2$ and $AO_{1.5}$ could be defined proportionally to progresses of reactions (1-4) measured in terms of cation fractions that occur as the reaction products

$$\Delta H_{\mathrm{mix}} = \left(\left[\,^{7}\mathrm{A}\right] + \left[\,^{7}\mathrm{B}\right]\right)\Delta H_1 + \left(\left[\,^{8}\mathrm{A}\right] + \left[\,^{6}\mathrm{B}\right]\right)\Delta H_2 + 2\left[\,^{7}\mathrm{B}\right]\Delta H_3 + 2\left[\,^{7}\mathrm{A}\right]\Delta H_4. \quad (6)$$

We note that Eqn. 6 does not distinguish cationic sublattices, and, thus, does not distinguish SRO from LRO. In the context of the present study this drawback is considered to be of a minor importance, as the study maintains that the main thermodynamic distinction of phases appearing in $A_xZr_{1-x}O_{2-0.5x}$ systems is due to their different composition in terms of the cationic species, namely $^{6}$A, $^{7}$A, $^{8}$A, $^{6}$B, $^{7}$B and $^{8}$B. Differences in the thermodynamic stability occurring due distinctions between SRO and LRO of a given type are assumed to be small. For example, the enthalpy effects due to SRO and delta-phase-type LRO in $Y_xZr_{1-x}O_{2-0.5x}$ system measured at $x \sim 4/7$ appear to be indistinguishable within the uncertainty of solution calorimetry data [19]. On the other hand, conveniently, the deficiency of the model in distinguishing SRO from LRO allows us using LRO concepts to emulate SRO effects.

Certain combinations of reactions (1), (2), (3) and (4) are also important for the understanding of stability of certain ordering schemes. In systems with stable pyrochlore the value of $\Delta H_2$ is more negative than the value of $\Delta H_1$. Thus, one expects that the reaction

$$^{7}\mathrm{A} + {}^{7}\mathrm{B} = {}^{8}\mathrm{A} + {}^{6}\mathrm{B}, \quad (7)$$

which represents the difference of reactions (2) and (1), is also characterized by a negative enthalpy effect in such systems. Combining (1) with (4) and (1) with (3) one obtains the reactions

$$^{7}A + {}^{8}B = {}^{8}A + {}^{7}B, \quad (8)$$

$$^{6}A + {}^{7}B = {}^{7}A + {}^{6}B, \quad (9)$$

which are similarly expected to have negative enthalpy effects, noting that the sense of these reactions is consistent with the strain-driven association of a vacancy to the smaller cation B. The reactions (8) and (9) are particularly relevant for the domains of $0 \leq x \leq 0.5$ and $0.5 \leq x \leq 1$, where the average cation coordination numbers vary within the intervals of {7 - 8} and {6 - 7}, respectively.

*2.2. Entropy of mixing*

The progress of reactions (1-4) at a given temperature is counterbalanced by the entropy factor. Thus the thermodynamic evaluation requires knowledge of the entropy as a function of cation species fractions. A proper treatment of the effect of SRO onto the configurational entropy of a solid solution requires using sophisticated techniques such as the cluster variation method [21, 22] or the thermodynamic integration coupled with the Monte Carlo simulations [23]. An approximate treatment of SRO [24] assumes that effects of local restrictions on the entropy can be emulated by reducing the space available for cation or anion mixing, i.e. by limiting the mixing of chemically different particles to a subset of the total number of available sites. In this approach SRO is emulated as LRO. Presently, the approach [24] is adopted and is developed as follows. Instead of a unique model emulating a certain SRO restriction over the whole composition range, we consider several models differing in the type of SRO applicable to specific composition domains. Then we interpolate between these limiting models with the aid of variational parameters. The values of the variational parameters are then determined via the Gibbs free energy minimization.

*2.2.1. Model DF(6,7,8) for disordered defect fluorite.*

The first step in the development of the general model is the characterization of the high-temperature distribution, which is not yet affected by reactions (1-4). The ideal mixing model is not a good solution for the disordered phase. Developing such a model would require considering the whole range of coordination numbers ($0 \leq K \leq 8$) and the necessity of describing the order/disorder effect within the $AO_{1.5}$ endmember. These complications can be avoided by postulating a fairly high degree of vacancy-vacancy avoidance governing the high-temperature distribution. The vacancy disordering in $Y_2O_3$ occurs at ~2500 K [20]. Thus for practical applications, it is possible to consider an endmember that is characterized by an ordered distribution of vacancies. For this reason we consider a hypothetical $AO_{1.5}$ end-member with $A_2A_2O_6VV$ pyrochlore structure. In this structure vacancies occupy 8b and 8a sublattices. Together these sublattices build a BCC (body-centred cubic) sublattice within the anion lattice of $A(O,V)_2$ fluorite. By inserting of extra oxygen anions into this sublattice and by substituting of an equivalent amount of A cations with B cations one can gradually transform the $AO_{1.5}$ pyrochlore into the cubic fluorite-type $BO_2$. Note, that such a model implies a high degree of vacancy-vacancy avoidance. The nearest-neighbour distance in BCC corresponds to 3NN distance of the anionic lattice of fluorite, thus, when extra oxygen anions are introduced by substituting vacancies within the BCC sublattice, no V-V contacts at shorter than 3NN distances can possibly occur, and the coordination number of any cation remains within the interval {6-8}. This model is further referred to as DF(6,7,8).

The restriction for the vacancies to be located within the BCC sublattice greatly reduces the configurational entropy of O/V in DF(6,7,8) fluorite. The mixing occurs only over a quarter of the total anion sites. The concentration of vacancies within the BCC sublattice, $x$, is higher than the average vacancy concentration of $0.25x$ by a factor of 4, while the total number of sites over which the anions can mix decreases by a factor of 4. Therefore, the configurational entropy of anions (per four moles of cations, eight moles of anions) is written as

$$S_{\mathrm{O/V}}\ (\mathrm{DF}(6,7,8)) = -2R(x\ln x + (1-x)\ln(1-x)). \tag{10}$$

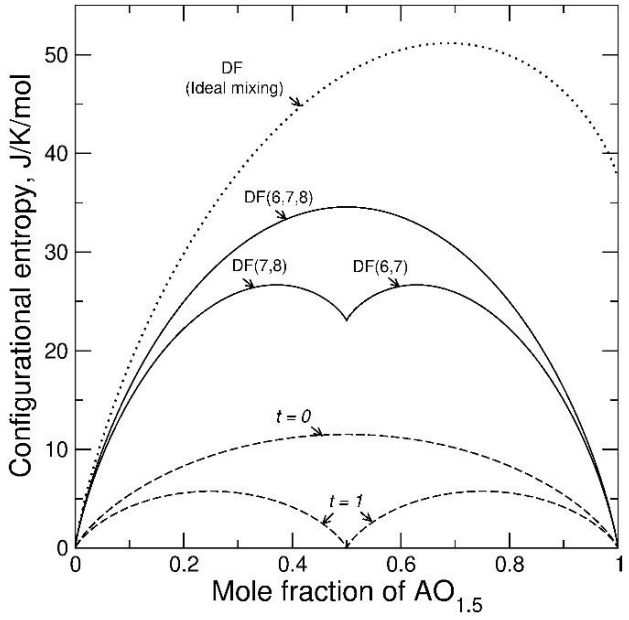


Fig. 1. Configurational entropy of the models DF(6,7,8), DF(7,8) and DF(6,7). The dashed curves show the entropy of anions within the imaginary BCC sublattice. The case $t = 0$ corresponds to DF(6,7,8), the case $t = 1$ corresponds DF(7,8) or DF(6,7) depending on the composition. The entropy of cations is added on top of the entropy of anions. The dotted line is the ideal mixing.

The cation fractions in DF(6,7,8) can be also worked out from the BCC model. Noting that any cation is surrounded (besides the other six 48f sites) by two anion sites belonging to the BCC sublattice, and that the concentration of vacancies in any BCC site is $x$, the fractions of 6-, 7- and 8-fold cations are proportional to the probabilities to find two, one or zero vacancies within the two BCC sites that are adjacent to a cation. These fractions are given in Table 1. Using these fractions the configurational entropy of cations (per four mole of cations) can be computed with the equation

$$S_{\mathrm{A/B\ (DF(6,7,8))}} = -4R\left(\begin{array}{l}\left[{}^{8}\mathrm{A}\right]\ln\frac{\left[{}^{8}\mathrm{A}\right]}{\left[{}^{8}\mathrm{A}\right]+\left[{}^{8}\mathrm{B}\right]}+\left[{}^{8}\mathrm{B}\right]\ln\frac{\left[{}^{8}\mathrm{B}\right]}{\left[{}^{8}\mathrm{A}\right]+\left[{}^{8}\mathrm{B}\right]}\\ +\left[{}^{7}\mathrm{A}\right]\ln\frac{\left[{}^{7}\mathrm{A}\right]}{\left[{}^{7}\mathrm{A}\right]+\left[{}^{7}\mathrm{B}\right]}+\left[{}^{7}\mathrm{B}\right]\ln\frac{\left[{}^{7}\mathrm{B}\right]}{\left[{}^{7}\mathrm{A}\right]+\left[{}^{7}\mathrm{B}\right]}\\ +\left[{}^{6}\mathrm{A}\right]\ln\frac{\left[{}^{6}\mathrm{A}\right]}{\left[{}^{6}\mathrm{A}\right]+\left[{}^{6}\mathrm{B}\right]}+\left[{}^{6}\mathrm{B}\right]\ln\frac{\left[{}^{6}\mathrm{B}\right]}{\left[{}^{6}\mathrm{A}\right]+\left[{}^{6}\mathrm{B}\right]}\end{array}\right). \tag{11}$$

Eqn. 11 assumes that the mixing could occur only between A and B cations which have the same coordination numbers. E.g. the mixing between $^{8}$A and $^{7}$B is not allowed because the swapping between these cations would cause a change in the cation species fractions and this would violate the model's constraint. The combined effect of Eqns. 10 and 11 is shown as the upper solid curve in Fig. 1. This function achieves the maximum at $x = 0.5$.

With the decrease in the temperature, progresses of reactions (1-4) are expected to affect the entropy. The entropy models are developed below for the domain of $0 \leq x \leq 0.5$. The models for the interval of $0.5 \leq x \leq 1$ are developed in the Supplementary Information File.

Table 1

Cation species fractions in DF(6,7,8) model ($0 \leq x \leq 1$)

| | |
|---|---|
| $^{8}$A | $x(1-x)^2$ |
| $^{7}$A | $2x^2(1-x)$ |
| $^{6}$A | $x^3$ |
| $^{8}$B | $(1-x)^3$ |
| $^{7}$B | $2(1-x)^2x$ |
| $^{6}$B | $(1-x)x^2$ |

*2.2.1. Transition from DF(6,7,8) to DF(7,8) ($0 \leq x \leq 0.5$).*

Within the $0 \leq x \leq 0.5$ domain the completion of reaction (1) leads to vanishing of $^{6}$A cations. This can be accomplished either via a migration of vacancies from A to B cations, or via a reduction of the total fraction of 6-fold cations. The second option is a more likely solution at high temperatures due to the entropy argument, as will be explained below. Model DF(7,8) corresponds to the limiting case of the simultaneous vanishing of $^{6}$B and $^{6}$A cations. Such a change in the spectrum of cation species (from the DF(6,7,8) state) could be viewed as a progressive increase in the degree of VV avoidance from the level of third neighbours (as in the BCC model) to the level of fourth neighbours. This extension of the

avoidance rule implies vanishing of 6-fold coordination of cations. An anion distribution with the avoidance of 3NN V-V pairs can be emulated by requesting vacancies to concentrate within a simple cubic sublattice, α, of the original anion lattice with the lattice parameter ($\boldsymbol{a}^* = 2\boldsymbol{a}$). The nearest neighbour distance within α is the 4NN distance in the original anionic lattice of fluorite. As the α sublattice is also a sublattice of BCC, the transition from DF(6,7,8) to DF(7,8) can be described as the ordering of vacancies into the α-subset of the BCC sublattice. A gradual transition from DF(6,7,8) to DF(7,8) can be described with a help of a variational parameter $t$, $0 \le t \le 1$, defining the concentration of vacancies in the α subset to be $P_\alpha = x(1+t)$. The concentration of vacancies in the other simple cubic subset of BCC, β, is then $P_\beta = x(1-t)$. The change in the entropy of the O/V distribution along the path from DF(6,7,8) to DF(7,8) is described with the function

$$S_{\mathrm{O/V}}\ (\mathrm{DF(6,7,8)} - \mathrm{DF(7,8)}) = -R(P_\alpha \ln P_\alpha + (1-P_\alpha)\ln(1-P_\alpha) + P_\beta \ln P_\beta + \big(1-P_\beta\big)\ln\big(1-P_\beta\big)) \ , \quad (12)$$

which is plotted in Fig. 1 in the disordered ($t$ = 0) and ordered ($t$ = 1) limits as dashed lines.

A progressive increase in the concentration of vacancies in the α sublattice implies a gradual change in cation fractions. These fractions could be computed by noting that each cation is surrounded by one α site and one β site. The fractions of 6-, 7- and 8-fold cations are then proportional to the probabilities of finding two, one and zero vacancies within these two sites (Table 2).

Table 2

Cation species fractions along the transition from DF(6,7,8) to DF(7,8) ($0 \le x \le 0.5$)

| | |
|---|---|
| [8]A | $x(1-P_\alpha))(1-P_\beta)$ |
| [7]A | $x(P_\alpha\,(1-P_\beta) + P_\beta\,(1-P_\alpha))$ |

| | |
|---|---|
| $^{6}$A | $xP_\alpha P_\beta$ |
| $^{8}$B | $(1-x)(1-P_\alpha))(1-P_\beta)$ |
| $^{7}$B | $(1-x)\,(P_\alpha\,(1-P_\beta)+P_\beta\,(1-P_\alpha))$ |
| $^{6}$B | $(1-x)P_\alpha P_\beta$ |

Note: $P_\alpha = x(1+t)$, $P_\beta = x(1-t)$, $0 \le t \le 1$.

The entropy of cations can be computed with Eqn. 11 using the cation fractions from Table 2. This function is added to the entropy of anions in Fig. 1. Notably, despite the change in the spectrum of cation coordination numbers the cation entropy remains constant along the transition from DF(6,7,8) to DF(7,8). This is because a decrease in the contribution from 6-fold cations automatically implies an equivalent increase in the contributions from 7- and 8-fold cations. This circumstance explains the entropy advantage of DF(7,8) type ordering as a response to reaction (1).

*2.2.2. Transition from DF(7,8) to DF1 ($0 \le x \le 1/3$).*

The further ordering within the $0 \le x \le 0.5$ interval can be attributed to the reaction (8). Depending on the composition, this reaction can lead to a complete vanishing of either $^{7}$A or $^{8}$B cations. These variants lead to the models DF1 ($0 \le x \le 1/3$) and DF2 ($1/3 \le x \le 1/2$), respectively, which were discussed in detail in [8]. The sense of reaction (8) is the redistribution of a vacancy between A and B cations. Thus, the ordering effect can be understood within the concept of a conditional probability, i.e. the probability of a cation, which is known with certainty to be either A- or B-type, to have a given coordination number. In the case of DF(7,8) the matrix of conditional probabilities has four elements, namely $p_{\mathrm{A}}^{7}$, $p_{\mathrm{A}}^{8}$, $p_{\mathrm{B}}^{7}$, $p_{\mathrm{B}}^{8}$. Particularly, the subset $p_{\mathrm{A}}^{7}$, $p_{\mathrm{A}}^{8}$ determines the probabilities for a cation A to be found in 7- and 8-fold coordination, respectively. The conditional probabilities satisfy the relationships of the type $xp_{\mathrm{A}}^{7} = [\,^{7}\mathrm{A}]$ and $(1-x)p_{\mathrm{B}}^{7} = [\,^{7}\mathrm{B}]$. From cation fractions of DF(7,8) model (Table 2, $t = 1$) one obtains $p_{\mathrm{A}}^{7} = p_{\mathrm{B}}^{7} = 2x$ and $p_{\mathrm{A}}^{8} = p_{\mathrm{B}}^{8} = 1-2x$. The equal conditional probabilities for A and B cations mean that in DF(7,8) there is no preference for cations A and B to have a specific coordination number. Destroying this equality

allows the description of the vacancy/cation association. A continuous transition from DF(7,8) to DF1 is defined here with the aid of the variational parameter $r_1$ , $0 \le r_1 \le 1$, requiring $p_{\mathrm{A}}^7 = 2xr_1$. The cases of $r_1$ = 1 and $r_1$ = 0 correspond to the limits DF(7,8) and DF1, respectively. The other conditional probabilities are computed from the relationship that links cation fractions to the average coordination number

$$\sum_{K=7}^{8} K\,([{}^{K}\mathrm{A}] + [{}^{K}\mathrm{B}]) = 7xp_{\mathrm{A}}^7 + 8xp_{\mathrm{A}}^8 + 7(1-x)p_{\mathrm{B}}^7 + 8(1-x)p_{\mathrm{B}}^8 = 8 - 2x\ , \qquad (13)$$

which has been introduced in [8]. The cation fractions as functions of $x$ and $r$ are given in Table 3. The configurational entropy of cations is then computed with Eqn. 11. Note, that the transition from DF(7,8) to DF1 implies a dramatic decrease in the cation entropy particularly at $x$ = 1/3 (Fig. 2). Effectively, at $x$ = 1/3 the solid solution is composed exclusively of $^7$B and $^8$A cations, while their contribution to the entropy of mixing is zero because of the difference in the coordination numbers.

Table 3

Cation species fractions along the transition from DF(7,8) to DF1 ($0 \le x \le 1/3$)

| | |
|---|---|
| $^8$A | $x(1 - 2xr_1)$ |
| $^7$A | $2x^2r_1$ |
| $^6$A | 0 |
| $^8$B | $1 - 3x + 2x^2r_1$ |
| $^7$B | $2x(1 - xr_1)$ |
| $^6$B | 0 |

Note, $0 \le r_1 \le 1$. The transition from DF(7,8) to DF1 does not imply any additional constraint onto the anion/vacancy distribution, because the average cation coordination does not change remaining within the interval of {7-8} in the both models. The entropy of anions in DF1 is the same as in DF(7,8) model.

*2.2.3. Transition from DF(7,8) to DF2 (1/3 ≤ x ≤ 1/2).*

When $1/3 \leq x \leq 1/2$ the completion of reaction (8) leads to vanishing of the fraction of $^{8}$B. A gradual transition from DF(7,8) to DF2 is defined, requesting the conditional probability $p_{\mathrm{B}}^{8}$ to vary as $p_{\mathrm{B}}^{8} = (1-2x)r_2$ , $(0 \leq r_2 \leq 1)$, The case of $r_2 = 0$ then corresponds to the complete extinction of $^{8}$B, which is the main constraint of DF2 [8]. The other conditional probabilities are computed from Eqn. 13. The cation fractions are given in Table 4.

Table 4.

Cation species fractions along the transition from DF(7,8) to DF2 ($1/3 \leq x \leq 1/2$)

| | |
|---|---|
| $^{8}$A | $(1-2x)(1-(1-x)r_2)$ |
| $^{7}$A | $3x-1-(1-2x)(1-x)r_2$ |
| $^{6}$A | 0 |
| $^{8}$B | $(1-x)(1-2x)r_2$ |
| $^{7}$B | $(1-x)(1-(1-2x)r_2)$ |
| $^{6}$B | 0 |

Note, $0 \leq r_2 \leq 1$.

The configurational entropy of cations is computed with Eqn. 11, while the entropy of anions is the same as in DF(7,8) model. Note, that at $x = 1/3$ and $r_2 = 0$ the DF2 model predicts zero entropy of mixing of cations. Over the interval of $1/3 \leq x \leq 1/2$ the entropy of cations increases rapidly due to the increase in the fraction of $^{7}$A allowing for the mixing between $^{7}$A and $^{7}$B (Fig. 2). In the limit of $r_2 = 0$ (DF2) the cation fractions are consistent with the derivation made in [8].

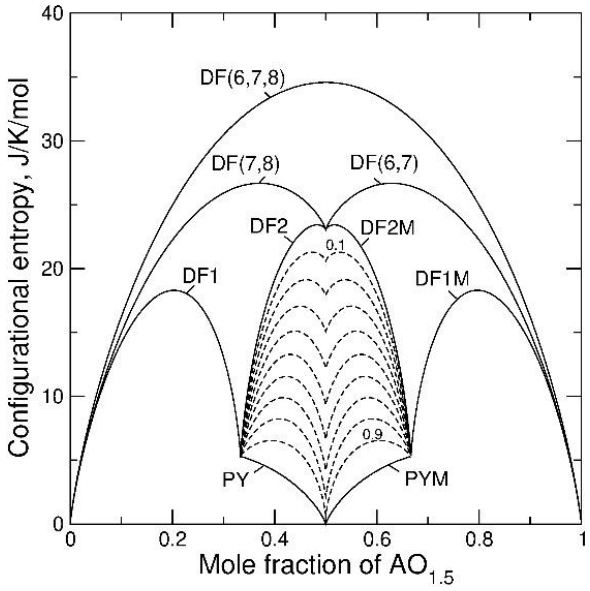


Fig. 2. Configurational entropies of all models used to simulate defect fluorite and pyrochlore phases. The dashed lines show isopleths of equal variational parameters $q$ and $q$' in the DF2/PY and DF2M/PYM transition models. The entropy values are per four moles of cations.

### *2.2.4. Transition from DF2 to PY ($1/3 \leq x \leq 1/2$).*

In systems with $\Delta H_2 < \Delta H_1$ the cation and anion distributions can further evolve due to the progress of reaction (7), i.e. the difference of reactions (2) and (1). Over the interval $1/3 \leq x \leq 1/2$ the completion of reaction (7) implies $[^7\mathrm{A}] = 0$. The reaction progress can be defined with the help of the variational parameter $q$ such that $[^7\mathrm{A}] = (3x - 1)(1 - q)$. The case of $q = 1$ corresponds to the PY model, while the case of $q = 0$ corresponds to DF2 model. The fractions of the other cations are worked out noting that a decrease in $[^7\mathrm{A}]$ must be consistent with an equivalent decrease in $[^7\mathrm{B}]$, while the fractions $^8\mathrm{A}$ and $^6\mathrm{B}$ are increased by the same amounts. The cation fractions are given in Table 5.

Table 5

Cation species fractions along the transition from DF2 to PY ($1/3 \leq x \leq 1/2$)

| | |
|---|---|
| $^8\mathrm{A}$ | $1 - 2x + (3x - 1)q$ |
| $^7\mathrm{A}$ | $(3x - 1)(1 - q)$ |

| | |
|---|---|
| $^{6}$A | 0 |
| $^{8}$B | 0 |
| $^{7}$B | $1 - x - (3x - 1)\, q$ |
| $^{6}$B | $(3x - 1)q$ |

Note, $0 \leq q \leq 1$.

The DF2-PY transition causes the reappearance of the 6-fold coordination. This implies a change in the ordering scheme of vacancies. DF2 model assumes the avoidance of V-V contacts at the first, second and third-neighbour distances. Such a distribution is emulated here by requiring vacancies to occupy the simple cubic sublattice α of the BCC sublattice. The SRO of PY-type implies reordering of vacancies into a different subset of BCC, which is assumed here to coincide with the 8b sublattice of pyrochlore. Note that the BCC sublattice could be split either into two simple cubic sublattices α and β, or into 8a and 8b sublattices of the pyrochlore structure, where each of these sublattices contain 1/8 of the total anion sites. As all these sublattices are of equal size, a redistribution of vacancies from α sublattice into 8b sublattice should not cause a significant change in the entropy of anions. Thus we associate no additional effect of anion ordering with the DF2/PY transition. The change in the entropy of cations is, however, significant. The entropy change along the DF2/PY transition can be computed with Eqn. 11 using the cation fractions from Table 5. Fig. 2 shows that an increase in the value of $q$ causes a rapid decrease in the entropy of cations particularly at $x = 0.5$. This is a consequence of the dramatic change in the spectrum of cation coordination numbers. The $^{6}$B and $^{8}$A cations, which occur as the products of reaction (7), cannot mix with each other.

*2.2.5. Long-range order in pyrochlore.*

The entropy model of DF2/PY transition can be developed further by taking into account long-range ordering in pyrochlore. LRO implies a not equal distribution of cations and anions over sublattices. In pyrochlore vacancies reside within the 8b sublattice that contains 1/8 of the total anion sites. Eqn. 12 ($t$ =

1) obviously suits to describe this ordered distribution, if the indices α and β are used to denote 8b and 8a sublattices. Here we make an assumption that both SRO and LRO of anions of PY-type can be modelled with the same Eqn. 12 constrained by $t = 1$. The transition from pyrochlore-type distribution to DF2-type distribution can be understood as a gradual shift of vacancies from 8b to α sublattice. As both sublattices contain equal amount (1/8-th) of anion sites, this transition implies no (little) change in the entropy of anions. LRO of pyrochlore type means that the cation distribution is split over two sublattices, which are denoted here as γ and δ. An unequal partitioning of cations over these sublattices is modelled with the aid of an additional parameter $Q$, $0 \le Q \le 1$ as shown in Table 6. The entropy of each sublattice can be still computed with Eqn. 11 rescaled to one half of available sites. The total entropy per four moles of cations is counted as the sum of the entropies of the sublattices. At $x = 0.5$ and $Q = 1$ the entropy of cations is zero. In the case of $Q = 1$ and $q = 0$ the sublattices are occupied by $^{7}$A and $^{7}$B, respectively, while in the case of $Q = 1$ and $q = 1$ the sublattices are occupied by $^{8}$A and $^{6}$B, respectively. Both these distributions correspond to zero entropy. The first case corresponds to the ordered stoichiometric fluorite (see Supporting Information in [8] for the description of the ordering scheme), the second one corresponds to the ordered stoichiometric pyrochlore. The problem of the present enthalpy model is that it gives no advantage to LRO over SRO. Thus, the states with $Q > 0$ cannot be made stable. To make the model formally consistent with crystallographic data, we artificially stabilise the long-range distribution by requiring $Q = q$. In effect, the minimization with respect to $q$, $0 \le q \le 1$, then formally describes a transition from short-range ordered DF2-like states to long-range ordered pyrochlore-like states.

Table 6

Cation species fractions along the transition from DF2 to PYLRO ($1/3 \le x \le 1/2$)

| | $^{8}$A | $^{7}$A | $^{7}$B | $^{6}$B |
|---|---|---|---|---|
| γ | $1 - 2x + w(1-Q)q$ | $w(1+Q)(1-q)$ | $1 - x - w + w\,(1-Q)(1-q)$ | $w(1+Q)q$ |
| δ | $1 - 2x + w(1+Q)q$ | $w(1-Q)(1-q)$ | $1 - x - w + w\,(1+Q)(1-q)$ | $w(1-Q)q$ |

Note: $w = 3x - 1$, $0 \le q \le 1$, $Q = q$.

*2.3. Gibbs free energy of mixing*

The entropy models described above together with analogous models for the interval of $0.5 \leq x \leq 1$ (see Supplementary Information File) are combined with Eqn. 6 to define the Gibbs free energies of four phases. The first phase, P1, ($0 \leq x \leq 1$) is characterized by the highest entropy uniting the models DF(6,7,8), DF(7,8) and DF(6,7) and all states of intermediate degree of order defined with the parameters $t$ and $t'$ ($0 \leq t, t' \leq 1$), where $t$ and $t'$ are relevant for $0 \leq x \leq 0.5$ and $0.5 \leq x \leq 1$ intervals, respectively. The second phase, P2, ($0 \leq x \leq 0.5$) unites the models DF(7,8), DF1 and DF2 and all states of intermediate order that are characterized by the variational parameters $r_1$ ($0 \leq x \leq 1/3$) and $r_2$ ($1/3 \leq x \leq 1/2$). The third phase, P2M, ($0.5 \leq x \leq 1$) unites the models DF(6,7), DF1M and DF2M together with all states of intermediate order characterized by the parameters $r_1$' and $r_2$' (see Supplementary Information File for the description of DF1M and DF2M). The last phase, P3, ($1/3 \leq x \leq 2/3$) unites the models DF2, DF2M, PY and PYM including all states of intermediate order characterized by the variational parameters $q$, $0 \leq q \leq 1$ ($1/3 \leq x \leq 1/2$) and $q'$, $0 \leq q' \leq 1$ ($1/2 \leq x \leq 2/3$). The non-equilibrium Gibbs free energy of mixing is computed for each of these phases by combining the relevant enthalpy of mixing and entropy of mixing terms according to the equation

$$\boldsymbol{\Delta G_{mix}(z,T,x) = \Delta H_{mix} - T\Delta S_{mix}}, \quad (14)$$

where $z = \{t, t', r_1, r_2, r_1', r_2', q, q'\}$ denotes the relevant variational parameter. Note that because of symmetric relationship between models defined for $0 \leq x \leq 0.5$ and $0.5 \leq x \leq 1$ intervals, the parameters $t$ and $t'$, $r_1$ and $r_1'$, $r_2$ and $r_2'$, $q$ and $q'$ are mathematically equivalent to each other, however, their equilibrium values may differ upon the free energy minimization due to the asymmetry inherent in the enthalpy equation. The evaluation of $\boldsymbol{\Delta H_{mix}}$ and $\boldsymbol{\Delta S_{mix}}$ terms requires the knowledge of cation speciation (this information is given in Tables 1-6). Moreover, $\boldsymbol{\Delta H_{mix}}$ depends on four energetic parameters $\boldsymbol{\Delta H_1}$, $\boldsymbol{\Delta H_2}$, $\boldsymbol{\Delta H_3}$ and $\boldsymbol{\Delta H_4}$. The equilibrium Gibbs free energy for each phase is obtained via the minimization

of the non-equilibrium Gibbs free energy with respect to the relevant variational parameter. The phase, which provides the lowest equilibrium free energy represents the final equilibrium state.

The developed hierarchical ordering scheme composed of the four phases provides a continuous description of the non-equilibrium enthalpy and entropy of mixing. In this construction all phases are linked together through common boundary (limiting) models. For example, the model DF(7,8) is the limiting model common to P1 and P2, while the model DF2 is the limiting model common to P2 and P3. The advantage of this modelling scheme is that only one variational (order) parameter is required for each phase at a given composition, and that the parameters belonging to different phases can be varied independently of each other. The final equilibrium Gibbs free energy is combined of the equilibrium Gibbs energies of phases that give the lowest energies at each given composition without an account for miscibility gaps. The final free energy can be further analysed with the common tangent method to outline miscibility gaps.

## 3. Results

The simulations are performed here for three sets of energetic parameters (Table 7), where each set comprises the values of $\Delta H_1$, $\Delta H_2$, $\Delta H_3$ and $\Delta H_4$. Set 1 illustrates phase equilibrium in an a $A_xB_{1-x}O_{2-0.5x}$ system, in which pyrochlore is a stable phase below and above the typical synthesis interval of 1673-1873 K. Calorimetric data for $Sm_xZr_{1-x}O_{2-0.5x}$ [25] were used as guides for the selected values. Set 2 models a system in which pyrochlore is stable just at and below the synthesis temperature. The data for $Gd_xZr_{1-x}O_{2-0.5x}$ and $Gd_2Hf_2O_7$ systems [14, 25] were used as the guide for constraining the parameters. The third set is chosen to represent a system in which pyrochlore is unstable well below the temperature of synthesis. The experimental data for $Y_xZr_{1-x}O_{2-0.5x}$ [19] and $Dy_xZr_{1-x}O_{2-0.5x}$ [25] guided the selected values of $\Delta H_1$, $\Delta H_2$, $\Delta H_3$ and $\Delta H_4$.

Table 7.

Enthalpies of reactions (1-4) in kJ/mol used as constraints for the enthalpy of mixing

| Set | $\Delta H_1$ | $\Delta H_2$ | $\Delta H_3$ | $\Delta H_4$ |
|---|---|---|---|---|
| 1 | –40 | –80 | –5 | 5 |
| 2 | –40 | –70 | –5 | –5 |
| 3 | –40 | –65 | –5 | –10 |

*3.1. System with pyrochlore stable below and above the synthesis temperature.*

One of the main characteristic features of the solution calorimetry data on a variety of $A_xB_{1-x}O_{2-0.5x}$ systems [19, 25, 26], B = {Zr, Hf}, A={Sm, Gd, Dy, Y}, is the strongly negative enthalpy of mixing in the disordered defect fluorite phase, which is computed relative to hypothetical cubic fluorite type endmembers $BO_2$ and $AO_{1.5}$. In the cases of A={Sm, Eu, Gd} the enthalpy of ordered pyrochlore is known [27] to be more negative than the enthalpy of the disordered phase at $x$ = 0.5. This behaviour could be predicted by choosing strongly negative values of $\Delta H_1$and $\Delta H_2$. The values of –40 and –80 kJ/mol were found to simultaneously fit the value of 2323 K of the order/disorder transition in Sm-pyrochlore [28] and the experimental data of Simoncic and Navrotsky [25] on the enthalpy of mixing in $Sm_xZr_{1-x}O_{2-0.5x}$ system under the assumption that that some of the data points correspond to the pyrochlore phase.

To compare the simulated isotherms with the experimental data, we assumed the enthalpy of the monoclinic to cubic transition in $ZrO_2$ to be 38.8 kJ/mol (per four moles of cations), as obtained by Lee et al. [19]. The enthalpy change due to the C-type to cubic (pyrochlore-type) transition in $SmO_{1.5}$ was assumed to be 90 kJ/mol (per four moles of cations). With the value of 90 kJ/mol four samples from the study of Simoncic and Navrotsky [25] fell very closely to the predicted 1673 and 1873 K isotherms (Fig. 3). The data representation is improved upon including a slight asymmetry introduced via different values of $\Delta H_3$and $\Delta H_4$.

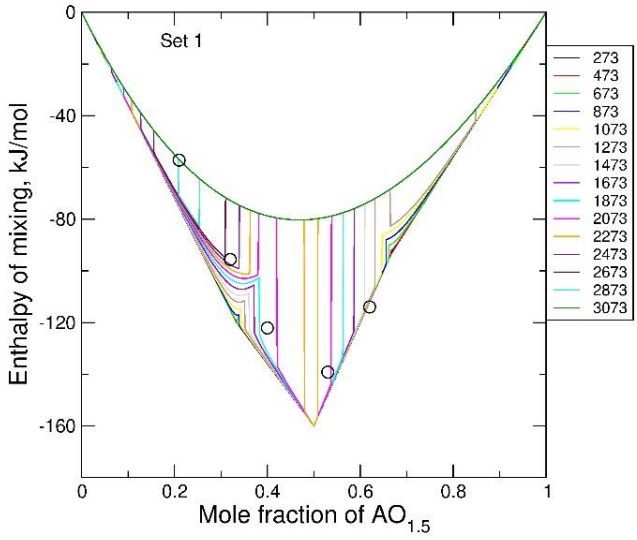


Fig. 3. Enthalpy of mixing in a system with pyrochlore stable below and above the temperature of synthesis constrained by the first set of parameters (Table 7). Lines are the enthalpy isotherms. Circles show the solution calorimetry data of Simoncic and Navrotsky [25] for $ZrO_2$-$SmO_{1.5}$ system plotted relative to hypothetical fluorite-type $ZrO_2$ and pyrochlore-type $AO_{1.5}$. The enthalpy of monoclinic to cubic transition in $ZrO_2$ and of C-type/pyrochlore transition in $AO_{1.5}$ are assumed to be 38.8 kJ/mol and 90 kJ/mol, respectively (per four moles of cations).

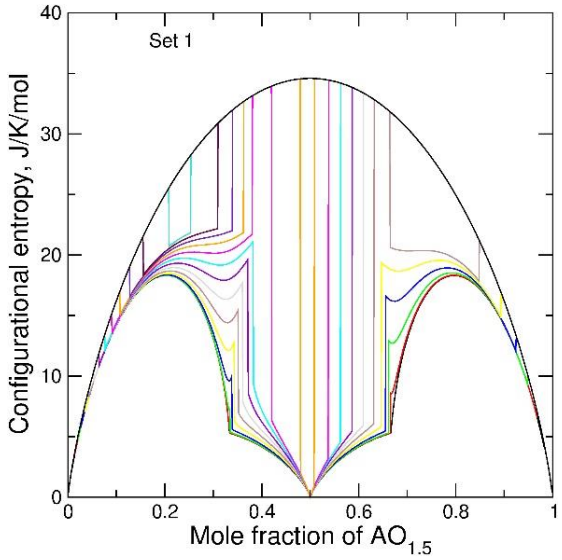


Fig. 4. Entropy of mixing in a system with stable pyrochlore constrained by Set 1 (Table 7). The colour code of the isotherms is the same as in Fig. 3.

The entropy plot (Fig. 4) shows that the transition at $x \sim 0.5$ occurs from the ordered pyrochlore ($q \sim 1$) to the defect fluorite, DF(6,7,8) with $t \sim 0$. The entropy effect is ~35 J/mol/K. This value is smaller than that offered by the ideal mixing model. The model predicts even smaller entropy and enthalpy effects at $x$

~ 0.37, where pyrochlore disorders into a DF2-type solid solution. The type of ordering along and isotherm could be guessed by comparing the entropy values along the isotherm to the Fig. 2, which shows the entropy frame of all models.

In Part I [8] we have shown that the experimental *a* vs. *x* data can be fitted under the assumption that pyrochlore-type solid solution directly transforms into DF1-type solid solution at $x \sim 1/3$. The present temperature-dependent modelling suggests an important modification to this scheme. The simulations show that the transition occurs first as the PY/DF2 type at $x \sim 0.37$, while upon the further decrease in *x*, the cation distribution in the disordered phase gradually evolves towards DF1-like scheme of SRO. Even in systems with stable pyrochlore the composition of $x \sim 1/3$ corresponds to a wending point between DF2-like and DF1-like schemes of order. A direct PY/DF1 transformation at $x \sim 1/3$ is precluded at elevated temperatures because of a too low entropy that is predicted with the DF1 model at $x \sim 1/3$.

A different interpretation of the wending point at $x \sim 1/3$ rises a question of the validity of the results of fitting of *a* vs. *x* data made in [8]. To test the accuracy of the cation radii and of the effective vacancy size determined in [8] we have directly computed isotherms of *a* vs. *x* in $ZrO_2$-$SmO_{1.5}$ system using the values of the cation and anion radii taken from Table 5 in Part I [8]. The results are shown in Fig. 5. To amplify differences between the model and the experiment, the linear Vegard law relation is subtracted from the data and from the isotherms. The plot shows that despite the simplified modelling scheme used in Part I in fitting the data, the cation and anion radii assesses in [8] still do a good job in representing the data in *a*-*x*-*T* space. This good representation benefits from the very similar *a* vs. *x* relationships predicted with DF1 and DF(7,8) models within the range of $0 \leq x \leq 1/3$.

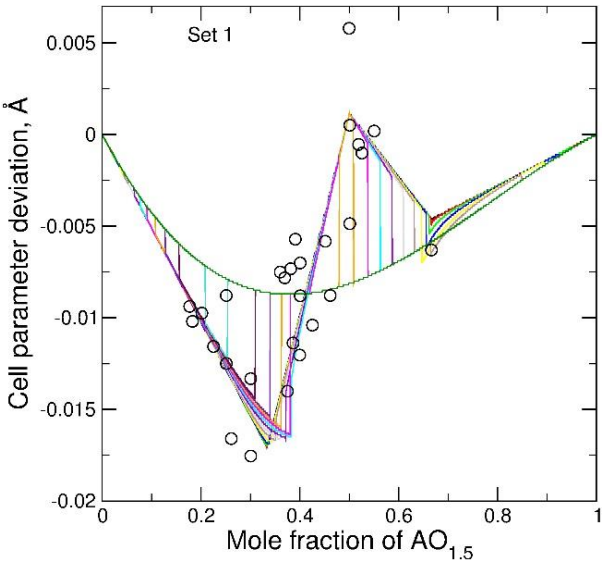


Fig. 5. Deviation of the cell parameter, *a*, (Å) at equilibrium at a given temperature from Vegard law relationship predicted with Set 1 (Table 7). Circles are the experimental data [29-32] on $Sm_xZr_{1-x}O_{2-0.5x}$ solid solution. The colour code of the isotherms is the same as in Fig. 3.

*3.2. System with pyrochlore marginally stable at the synthesis conditions.*

Set 2 (Table 7) illustrates a system in which the pyrochlore/fluorite transition happens close to the temperature of the synthesis (1673-1873 K). It is known that $Gd_2Zr_2O_7$ compounds can be synthesized both in ordered and disordered forms depending on the temperature and quenching rate [33]. The data analysis of Saradhi et al. [15] suggests that the enthalpy difference between the ordered and disordered phases decreases linearly with the decrease in the radius of A cation, while the formation enthalpy of the disordered phase is more or less independent on this parameter. The change from $Sm_xZr_{1-x}O_{2-0.5x}$ type to $Gd_xZr_{1-x}O_{2-0.5x}$ type of thermodynamic behaviour can thus be simulated by making $\Delta H_2$ value less negative than in Set 1, while keeping the value of $\Delta H_1$ unchanged. The value of $\Delta H_3$ was fixed at the value of 5 kJ/mol as in Set 1 because this parameter cannot depend on the type of A cation. The value of $\Delta H_4$ was then constrained by Eqn. 5. The parameter of $\Delta H_2$ = –70 kJ/mol was set as a compromise value, which simultaneously fitted the calorimetric data of Simoncic and Navrotsky [25] on disordered $Gd_xZr_{1-x}O_{2-0.5x}$ samples and predicted a reasonable temperature of the order-disorder transition of ~1673 K at $x \sim 0.5$.

The interesting feature of the enthalpy plot (Fig. 6) is that at most of the relevant temperatures the transition occurs between the ordered pyrochlore and the disordered DF2-type solid solution. The DF(6,7,8)-type distribution is predicted only within a limited range of compositions close to $x \sim 0.5$. This happens because Set 2 enhances the stability of the partially ordered P2 phase relative to the pyrochlore phase. The consequence is that the enthalpy and entropy effects of the order/disorder transition are greatly reduced relative to values predicted with the Set 1. This tendency is consistent with the experimental observations [14, 15]. Importantly, the consistency with the enthalpy of disordering data is obtained together with a very reasonable order/disorder transition temperature of ~1673 K. This becomes possible due to the reduced values of the entropy effects. The model predicts that the transition occurs between the essentially ordered pyrochlore and the DF2-type solid solution. This observation can be made by comparing the equilibrium entropy isotherms (See Fig. S1 in the Supplementary Information File) with Fig. 2.

Fig. 8 shows *a* vs. *x* isotherms in the $Gd_xZr_{1-x}O_{2-0.5x}$ solid solution. The experimental data, which correspond to the interval of $0.33 \leq x \leq 0.6$, are consistent with the pyrochlore ordering. Although the model predicts DF2-type states to be stable at about the synthesis temperature, *a* vs. *x* data suggest that such states may not be well quenched in the $ZrO_2$-$GdO_{1.5}$ system.

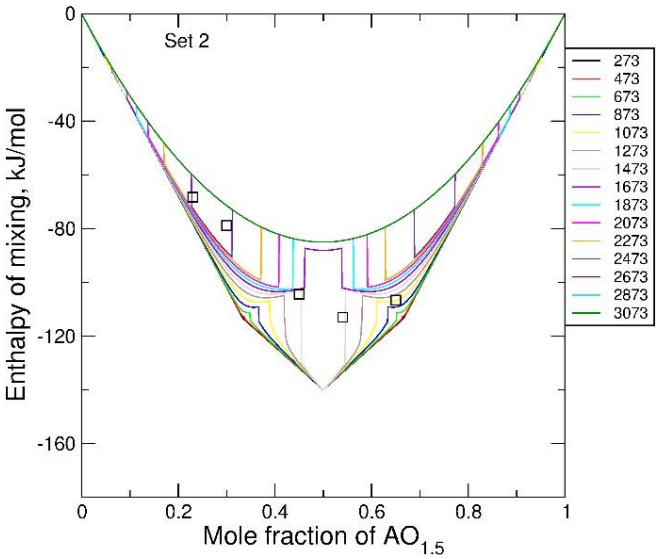

Fig. 6. Enthalpy of mixing in a system constrained by Set 2 (Table 7). Lines are the enthalpy isotherms. Squares show the solution calorimetry data of Simoncic and Navrotsky [25] for $ZrO_2$-$GdO_{1.5}$ system plotted relative to hypothetical fluorite-type $ZrO_2$ and pyrochlore-type $AO_{1.5}$. The enthalpy of monoclinic to cubic transition in $ZrO_2$ and of C-type/pyrochlore transition in $GdO_{1.5}$ are assumed to be 38.8 kJ/mol and 92.5 kJ/mol, respectively (per four moles of cations).

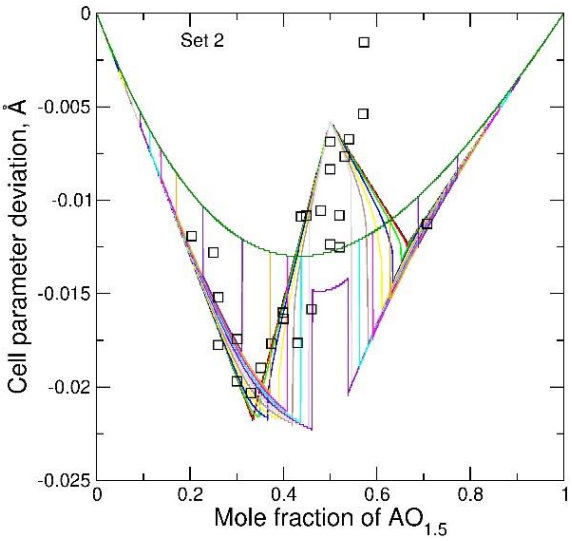


Fig. 7. Deviation of the cell parameter, *a*, (Å) at equilibrium at a given temperature from Vegard law relationship predicted with Set 2 (Table 7). Squares are the experimental *a* vs. *x* data [33-37] on $Gd_xZr_{1-x}O_{2-0.5x}$ solid solution. The colour code of the isotherms is the same as in Fig. 6.

### *3.3. System with defect fluorite stable below and above the synthesis temperature.*

Set 3 in Table 7 illustrates a system in which pyrochlore does not appear as a stable phase at any experimental conditions. The values of $\Delta H_1$, $\Delta H_2$ and $\Delta H_3$ parameters are again guided by the analysis of Saradhi et al. [15]. Eqn. 5 implies that the decrease in the absolute value of $\Delta H_2$ causes the decrease in the value of $\Delta H_4$. This effect makes a combination of P2 and P2M phases more stable than pyrochlore within a wide range of temperatures. Pyrochlore is predicted as a stable phase only below 773 K. The calorimetric data [19, 25] on $Y_xZr_{1-x}O_{2-0.5x}$ and $Dy_xZr_{1-x}O_{2-0.5x}$ systems are consistent with the DF2-like distribution at intermediate compositions and with DF1-like distribution at more diluted compositions (Fig. 8). The configurational entropy plot (Fig. S2 in the Supplementary Information File) shows that the isotherms which correspond to typical conditions of the synthesis (1673, 1773 and 1873 K) lie close to DF(7,8)

states, while DF1- and DF2-like ordering is predicted at much lower temperatures. On the other hand, most of *a* vs. *x* data on $Y_xZr_{1-x}O_{2-0.5x}$ and $Dy_xZr_{1-x}O_{2-0.5x}$ systems fall below the 1673K isotherm (Fig. 9 and Fig. S3) suggesting that the cation distributions in most of the samples may have evolved to DF1- and DF2-like ordering states during slow quenching. The more disordered distribution of the samples used in the calorimetric study [19] could possibly be explained under the assumption of a more rapid quenching. An interesting prediction is that at temperatures of ~1873 K particularly at $x \sim 0.5$ the entropy isotherms bend towards the DF(6,7,8) model suggesting the admixture of partially disordered states containing minor amounts of cations in 6-fold coordination. The $^{89}$Y MAS-NMR data of Kawata et al. [38] show the presence of 6-fold coordinated Y particularly at $x = 0.5$ and $x = 0.6$. At $x = 0.6$ the presence of $^{6}$A cations is consistent with DF(6,7) model, however, at $x = 0.5$ the presence of 6-fold coordinated Y implies the admixture of more disordered DF(6,7,8) states.

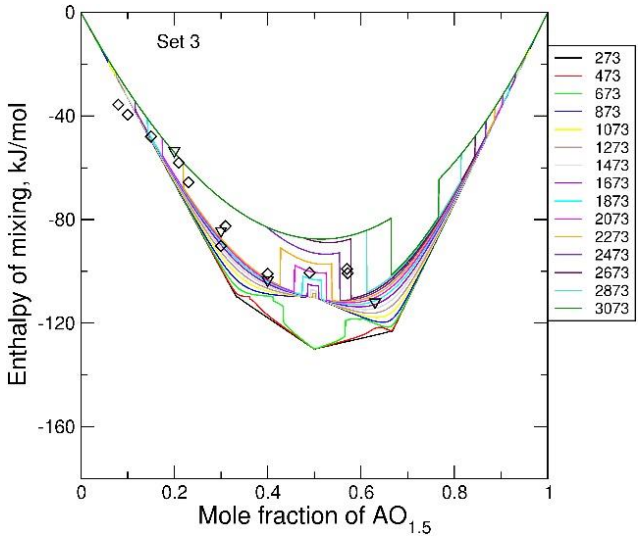


Fig. 8. Enthalpy of mixing in $ZrO_2$-$AO_{1.5}$ system constrained by Set 3 (Table 7). Lines are the enthalpy isotherms. Diamonds show the solution calorimetry data of Lie et al. [19] for $ZrO_2$-$YO_{1.5}$. Down triangles are the data of Simoncic and Navrotsky [25] for $ZrO_2$-$DyO_{1.5}$ system plotted relative to hypothetical fluorite-type $ZrO_2$ and pyrochlore-type $AO_{1.5}$. The enthalpies of C-type/pyrochlore transitions in $YO_{1.5}$ and in $DyO_{1.5}$ are assumed to be 110 kJ/mol and 100 kJ/mol, respectively (per four moles of cations).

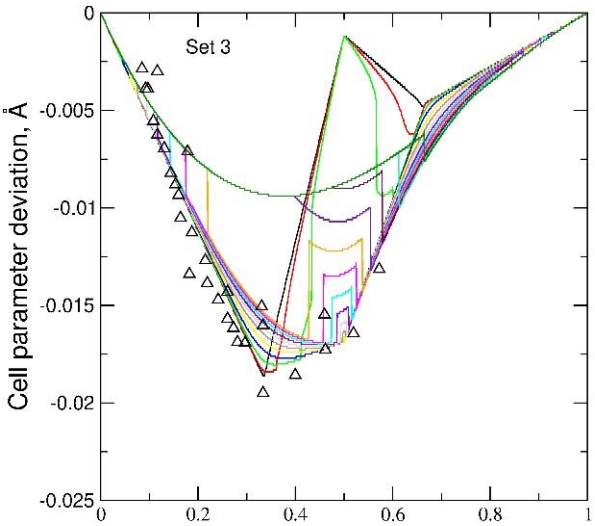


Fig. 9. Deviation of the cell parameter, *a*, (Å) at equilibrium at a given temperature from Vegard law relationship predicted with Set 3 (Table 7). Triangles are the experimental *a* vs. *x* data [39-42] on $Y_xZr_{1-x}O_{2-0.5x}$ solid solution. The colour code of the isotherms is the same as in Fig. 8.

### *3.4. Free energy of mixing and phase relations*

The free energy isotherms corresponding to the sets 1, 2 and 3 are shown in Figures S4, S5 and S6, respectively (see Supplementary Information File). Fig. S4 shows that in a system that is modelled with Set 1 pyrochlore remains as a stable phase up ~2273 K. Two-phase miscibility gaps develop at both sides of the pyrochlore field. This prediction is in good qualitative agreement with phase relations observed in $ZrO_2$ - $NdO_{1.5}$ and $ZrO_2$ - $SmO_{1.5}$ systems [44]. The main difference is that the miscibility gaps are predicted to be significantly wider. The change of parameters from Set 1 to Set 3 causes a progressive destabilization of pyrochlore relative to a mixture of two SRO phases, P2 and P2M. The P2M phase becomes progressively more stable relative to the P2 phase. The phase relations corresponding to set 3 would be qualitatively consistent with the phase diagram of $ZrO_2$ - $YO_{1.5}$, if the P2M phase is interpreted as the delta phase. Achieving this consistency would require an additional stabilization of the LRO scheme of delta phase relative to P2M specifically at the composition of $x \sim 4/7$. Such calculations cannot be performed within the postulates of the present model, where SRO and LRO effects are not distinguished.

*3.5. Optimal conditions for ionic conductivity*

In Part I [8] we have argued that the ionic conductivity of $A_xB_{1-x}O_{2-0.5x}$ solid solutions should benefit from vacancy migration events, in which the local strain energy remains the same before and after the swap. The condition of zero strain energy change was linked to the condition of the conservation of net cation coordination numbers. The latter condition is fulfilled when local cation configurations about the vacancy and the migrating oxygen anion before and after the swap are in a symmetric relationship to each other. We have assumed that in a DF1-type solid solution the strain energy conserving vacancy migration occurs through a continuous network formed by pairs of $B_4V$ and $B_4O$ clusters of tetrahedral shape sharing a common $B_2$ edge. Thus, the migration probability was assumed proportional to the occurrence probability of such a pair. We have also argued that the migration probability should be additionally proportional to the factor $x(1 – 2x)$, which follows from the preservation of vacancy-vacancy avoidance. The migration probability function was shown to achieve a maximum at $x \sim 0.146$.

The present temperature dependent simulations suggest, however, that the DF1 model is applicable only at low temperatures or low fractions of $AO_{1.5}$, while at elevated temperatures the cation distribution shifts towards the DF(7,8) model. Thus it appears important to investigate the cluster probabilities within the general DF(7,8)/DF1/DF2 model over the interval $0 \leq x \leq 1/2$. In this model the tetrahedral clusters split into $(^8B,^8A)_4X$, $X$ ={O,V] and $(^7B,^7A)_2(^8B,^8A)_2O$ types, implying that all vacancies are always inside the clusters of the first type. The vacancy swaps could occur only between $(^7B,^7A)_4V$ and $(^7B,^7A)_2(^8B,^8A)_2O$ clusters. Similarly to the already investigated DF1 model case, the condition of the local strain energy conservation occurs when these clusters are in $^7B_4V$ and $^7B_2{}^8B_2O$ configurations. The probabilities of finding $^8B$ and $^7B$ in $(^7B,^7A)_4V$ and $(^7B,^7A)_2(^8B,^8A)_2O$ clusters in the general DF(7,8)/DF1/DF2 model are $\frac{[\,^8B]}{[\,^8B]+[\,^8A]}$ and $\frac{[\,^7B]}{[\,^7B]+[\,^7A]}$, respectively. Thus, the probability of strain conserving migration is proportional to the factor $x(1-2x)\left(\frac{[\,^7B]}{[\,^7B]+[\,^7A]}\right)^4\left(\frac{[\,^8B]}{[\,^8B]+[\,^8A]}\right)^2$, where the cation species fractions are computed via the minimization of the free energy of the general DF(7,8)/DF1/DF2

model. This factor normalized by its maximum value at 273 K is plotted in Fig. 10. The temperature makes the probability function more dispersed towards larger values of *x*, however, the position of the maximum does not change significantly within the interval of 273-1073 K, thus the argument on the origin of maximum made in [8] remains valid with the more general model.

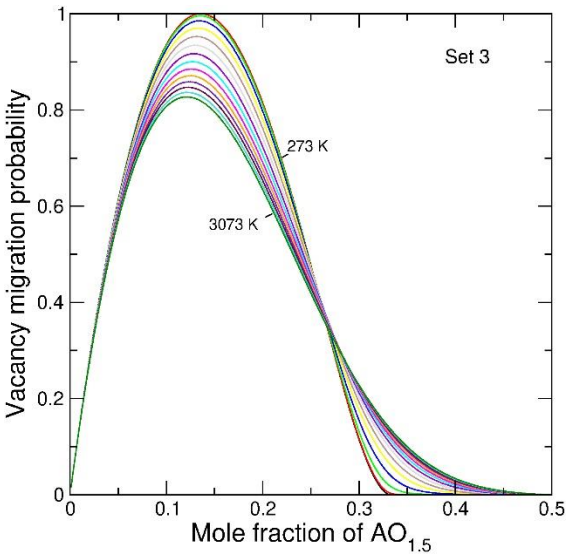


Fig. 10. Isotherms of normalized probability of strain energy conserved vacancy migration for an $A_xZr_{1-x}O_{2-0.5x}$ DF(7,8)-type solid solution predicted with Set 3. The decreasing temperature moves the distribution closer to DF1 and DF2 models. The pyrochlore-type ordering is suppressed.

### *3.5. Optimal conditions for radiation stability*

In Part I we hypothesized that the radiation stability benefits from maximization of cation species that occur with same coordination numbers. The elastic energy is thought to be mostly affected by swaps that lead to a change in cation coordination. Thus the maximisation of species of same coordination should be beneficial for the radiation stability. Trivially, within this hypothesis, the end-members $BO_2$ and $AO_{1.5}$ should correspond to local maxima in radiation stability as their structures are based on cations of same type. A non-trivial problem is the prediction of relative stability of solid solution phases. The relative stability of such phases could possibly be modelled with a function that grows with an increase in fractions of species with same coordination at a given value of *x*. It is also conceivable that the radiation stability

increases at a composition, in which swaps between cations occurring in same configurations can be achieved in a plethora of equivalent ways. Accidently, the configurational entropy of cations serves the purpose of representing such a function. Fig. 11 plots the entropy of cations. Based on this figure one can predict the solid solutions with the DF2-type distribution to have higher radiation stability relative to solid solutions with PY-type distribution. On the other hand, DF2- and DF1-type solid solutions with the compositions centred at $x \sim 1/3$ and $x \sim 2/3$ should be less stable relative to solid solutions with DF(7,8) and DF(6,7) distribution schemes. As the latter solid solutions are stabilized by the temperature factor, one can assume that the temperature affects the radiation stability not just through the agitation of atoms, but also through making the cation distributions less susceptible to defect energy accumulation.

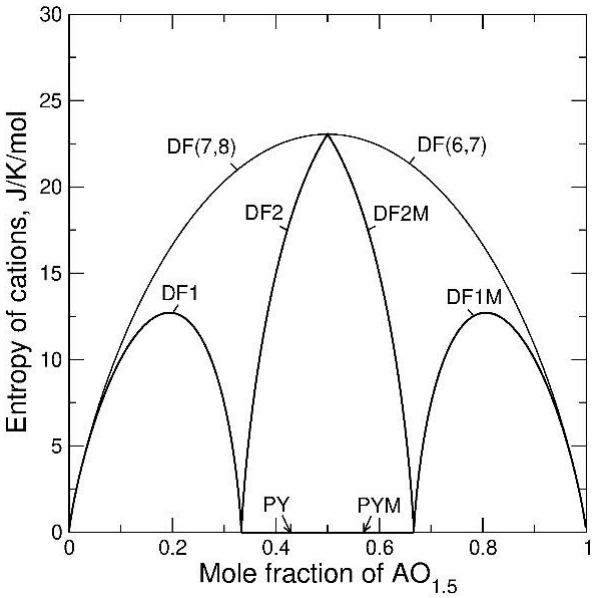


Fig. 11. Entropy of cations in the models discussed in the text. The entropy function in the model DF(6,7,8) coincides with the functions corresponding to models DF(7,8) and DF(6,7). Models PY and PYM have zero entropy. The entropy functions are thought to correlate with relative radiation stability of solid solutions with different schemes of order.

## 4. Discussion

A consistent description of calorimetric and structural data is achieved here with a model that assumes the presence in defect fluorite of a hierarchy of four schemes of anion and cation/anion order. The hierarchy

of ordering effects makes sense considering the different strength of interactions that drive the ordering. The strongest interactions are due to the electrostatic forces between the vacancies, the less strong are the strain-driven interactions between the anions and cations and the least strong interactions are those that require a compromise between anion-anion and cation-anion ordering tendencies [9,10]. The consistent description of calorimetric and structural data implies that at typical temperatures of synthesis the ordering due to the strongest anion-anion interactions is essentially complete. The observed variability in the thermodynamic behaviour of $A_xZr_{1-x}O_{2-0.5x}$ systems that is manifested by the temperature of P/DF transition is determined by less strong ordering effects that imply a compromise between anion-anion and cation-anion interactions.

One of the aims of the present thermodynamic modelling was to justify the ordering schemes, which were postulated in [8]. This aim is achieved. We show here that the DF1, DF2, PY, DF1M, DF2M and PYM models are thermodynamically sensible, representing ground states of a more general model. The schemes of SRO (or LRO) that underline these models can be thermodynamically stabilized by four parameters representing enthalpy effects of reactions (1-4) between cation species. The sum of the effects of reactions (1), (3) and (4) drives the ordering from DF(6,7,8) towards DF(7,8) and DF(6,7), the difference of the effects of reactions (1) and (4) drives the ordering from DF(7,8) towards DF1 and DF2, similarly, the difference of the effects of reactions (1) and (3) drives the ordering from DF(6,7) to DF1M and DF2M, while the difference of effects of reactions (2) and (1) drives the ordering from DF2 and DF2M to PY and PYM, respectively. The enthalpies of reactions (1) and (2) determine the magnitude of the ordering effects and the sequence of ordering transformations.

The study predicts negative enthalpies of mixing in the disordered solid solutions and reduced values of the entropy effects due to the order/disorder pyrochlore/fluorite transition consistently with the experiment. Importantly, the enthalpy isotherms that fit solution calorimetry data simultaneously reproduce the data on *a* vs. *x*. At the same time, the adopted values of the enthalpy effects of the reactions (1) and (2) are consistent with available solution calorimetry data. Particularly, the values of $\Delta H_1$ and $\Delta H_2$

are consistent with the analysis of solution calorimetry data on $A_2B_2O_7$ systems given by Saradhi et al. [15], under the assumption that disordered solutions are based on the combination of $^7$A and $^7$B species. Interestingly, the same assumption allows to link the calorimetric data to defect formation energies in pyrochlores. Indeed, the formation energy of cation antisite (CA) defect in pyrochlore corresponds to the effect of reverse reaction (2), while the formation of anion Frenkel pair (AFP) corresponds to twice the difference of reactions (1) and (2). Indeed, a swap of a vacancy from 8b into a neighbouring 48f site creates two $^7$B and two $^7$A cations from two $^6$B and two $^8$A cations. The defect formation energies have been recently computed with DFT by Li et al. [46] for pyrochlores covering a wide range of A and B cation radii. Consistently with the calorimetric data [15], the AFP formation energies [46] decrease monotonously in zirconate pyrochlores with the decrease in the radius of A cation changing their sign to negative when the radius of A becomes smaller than that of Nd [1]. Though, the calorimetric data show that the fluorite state is higher in the enthalpy for all studied zirconate pyrochlores. This suggests that the AFP formation energies calculated with DFT likely need to be adjusted (increased) by about 0.5 eV to yield the sign change not at $R_A \sim R_{Nd}$ , but at $R_A \sim R_Y$. A similar level of consistency is seen between the calorimetric data and the CA formation energies computed by Li et al. [46].

The present study reveals a more detailed scheme of transformations between the different types of ordering. In Part I we assumed that the transitions DF1/DF2 and DF1/PY always occur at $x = 1/3$ independently of the temperature. Here we show that this assumption can be justified only at low temperatures. The temperature dependent calculations suggest that samples with $0 \leq x \leq 1/3$ synthesized at ~1873 would unlikely develop pure DF1-type ordering. A more realistic model predicts higher degrees of disorder in the vicinity of $x = 1/3$. Particularly, the proposition made in [8] that the composition driven transition from defect fluorite to pyrochlore in all pyrochlore-type systems happens as a DF1/PY transformation requires a modification. Temperature dependent simulations suggest that at a typical synthesis temperature with the increase in $x$ the DF1-type solid solution first evolves towards the DF2-type cation distribution through DF(7,8)-like states, and then the DF2-type solid solution transforms into

the PY phase. The exact composition at which the transformation takes place is predicted to depend on the synthesis temperature. The main reason for the admixture of states with higher degrees of disorder at $x \sim 1/3$ is the minimum in the configurational entropy, which develops at this composition at low temperatures. When the temperature increases, a strong SRO at $x \sim 1/3$ becomes thermodynamically unfavourable. On the other hand, our calculations show that in the range of $0 \leq x \leq 1/3$ models DF1 and DF(7,8) are practically indistinguishable in terms of the predicted *a* vs. *x* dependences. This observation justifies the use of the simple DF1/PY model in fitting *a* vs. *x* data, as done in [8]. The temperature-dependent simulations unexpectedly predict that at a composition close to $x \sim 0.5$ pyrochore could directly disorder into DF(6,7,8)-like phase avoiding DF2-like distribution. This behaviour is seen in systems which have a strong tendency to the formation of pyrochlore. This could be a drawback of the simplified (LRO) entropy model for vacancy ordering in DF(6,7,8). This model assumes that vacancies are arranged over a hypothetical simple cubic sublattice with the lattice vector of $2\boldsymbol{a}$. At low temperatures and at $x = 0.5$ this assumption leads to zero entropy contribution from O/V mixing. In reality the short-range ordering of vacancies even at $x = 0.5$ can be realised in a plethora of different ways resulting in a larger entropy for DF2-type distribution, thus, making it more stable relative to DF(6,7,8).

The interesting question is how the presently developed thermodynamic model correlates with the weberite model of defect fluorite, which has been proposed in recent crystallographic studies [16, 17]. Within the present concept the weberite-type distribution at $x = 0.5$, $^{8}A^{6}B(^{7}A_{x}{}^{7}B_{1-x})_{2}O_{7}V$, could be understood as a result of an incomplete PY/DF2 transformation corresponding to $q \sim 0.5$. The present model does not predict such intermediate states as equilibrium states favouring an abrupt transition from PY-like, $^{8}A_{2}{}^{6}B_{2}O_{7}V$, to DF2-like, $(^{7}A_{x}{}^{7}B_{1-x})_{4}O_{7}V$, distribution. The main problem of stabilizing weberite within the present modelling frame, is its low configurational entropy, which is formally 2Rln2 per four cations at $x = 0.5$. The solution calorimetry data [15] and data on the temperature of the order/disorder transition [45] require a twice larger value. This larger entropy is met by the DF2 model. The observed uniformly good performance of the weberite model [16] could possibly be explained under the assumption

that structural differences between DF2, DF1 and weberite ordering schemes are not well resolved at the PDF level. Indeed, all these models comply with a high degree of vacancy-vacancy avoidance and a high or intermediate degree of B-cation-to-vacancy association. We conclude that the building of a model of defect fluorite that is consistent with both structural and thermodynamic data requires a further effort. The testing of DF1, DF2 and DF(7,8) models against neutron scattering data could be the next step towards this aim.

## 5. Conclusions

A hierarchical thermodynamic model of cation and anion ordering is developed and is shown to be consistent with calorimetric and structural data on defect fluorite and pyrochlore solid solutions. The main conclusion of the present study as well as of the connected study [8] is that a variety of structural, thermodynamic and physical properties of Zr-based fluorite and pyrochlore ceramics could be understood within the concept of constraints on cation coordination numbers. These constraints are introduced here with the help of the concept of cation species, which distinguishes cations not only through their chemical type and charge, but also through their coordination numbers. SRO and LRO constraints are set either as rigid postulates requiring certain types of cation species to vanish [8], or (in a more subtle way) thermodynamically by defining energies of reactions between cation species.

The changes in the enthalpy of mixing due changes in the composition and/or state of order are expressed proportional to progresses of the reactions (1-4) between cation species. These changes are accompanied by a reduction in the configurational entropy. The entropy is decreased, on the one hand, due to a reduction of anion sites available for vacancies, and, on the other hand, due to restrictions on mixing between cation species with different coordination numbers. Differences in the thermodynamic properties of $ZrO_2$-$AO_{1.5}$ systems, e.g. the relative stability of the pyrochlore phase, and different types of *a* vs. *x* relationships, can be attributed to the ratio of $\Delta H_2$ and $\Delta H_1$ parameters. Presumably, the value of

$\Delta H_2$ correlates with the difference in the radii of 8-fold A and 6-fold B cations. The stabilization of DF1 type ordering is attributed to the negative enthalpy effect of reaction (8), i.e. to the difference of the effects of reactions (1) and (4). The negative enthalpy fits with the concept of strain minimization via the association of small (B) cations with large vacancies and large A cations with oxygen anions.

The concept of DF1-type order may have an important implication to the mechanism of ionic conductivity in doped zirconia. The association of vacancies to B (Zr) cations restricts the majority of O/V swaps to a network of connected $B_4V$ and $B_4O$ clusters within which the transport of vacancies could occur without a net change in the spectrum of cation coordination numbers, avoiding states with high local strain [8]. Here the model [8] is extended to a more general model of DF(7,8)-DF1-DF2 ordering. It is shown that the more general model predicts a similar composition dependence of the relative conductivity, with the maximum at $x \sim 0.14$.

In an analogue with low-strain O/V swaps a concept of low-strain A/B cation swaps and cation Frenkel pair defect formation events has been proposed in [8]. Such swaps could be identified by counting net changes in cation coordination. This concept leads to a proposition that mixed compounds that maximize numbers of cation species with same coordination numbers should have superior resistance to the radiation induced amorphization. Here this concept is developed further by invoking the entropy argument. We argue that the radiation stability should be correlated with the number of microstates that are consistent with a given spectrum of cation coordination numbers. The larger the number of such microstates, the higher the probability that this spectrum will not be affected by a defect formation event. The prediction of relative radiation stability of a pair of structures with the same composition could thus be made by comparing their configurational entropies.

Further effort is needed in testing the model predictions and in extending the model to $BO_2$ - $AO_{1.5}$ systems with B = {Ti, Hf, Ce, Th, U} and A = {*Ln*, *An*}. We assume that the association of a vacancy to a B-type cation would be much less pronounced in systems with Ce, Th and U, while additional

complexities would be expected for Ce- and U-systems due to redox effects. Vacancy-vacancy avoidance constrains are expected to be relevant for all systems.

**Acknowledgements**

This work has been partially supported with funding from the German Federal Ministry for Education and Research (BMBF, grant 02NUK021A).

**Conflicts of interests**

There are no conflicts to declare.

**Contributions of the authors**

AAB developed the concept of constraints on cation coordination numbers in determining breaks in the variation of the lattice parameter of fluorite-type ceramics with composition. VLV further linked constrains on coordination numbers to effects of SRO and LRO in cation and anion distribution and developed a thermodynamic description of SRO and LRO.

**References**

[1] H. Yamamura H. Nishino, K. Kakinuma, K. Nomura, Electrical conductivity anomaly around fluorite-pyrochlore phase boundary, Solid State Ionics 158 (2003) 359-365

[2] J.A. Díaz-Guillén, A.F. Fuentes, M.R. Díaz-Guillén, J.M. Almanza, J. Santamaría and C. León, The effect of homovalent A-site substitutions on the ionic conductivity of pyrochlore-type $Gd_2Zr_2O_7$, J. Power Sources, 186 (2) (2009) 349-352

[3] R.C. Ewing, W.J. Weber, and J. Lian, Nuclear waste disposal-pyrochlore ($A_2B_2O_7$): Nuclear waste form for the immobilization of plutonium and "minor" actinides, J. Appl. Phys. 95 (2004) 5949-5971

[4] S. X. Wang, B. D. Begg, L. M. Wang, R. C. Ewing, W. J. Weber, and K. V. G. Kutty, Radiation stability of gadolinium zirconate: A waste form for plutonium disposition, J. Mater. Res. 14 (1999) 4470-4473

[5] J. Lian, X. T. Zu, K. V. G. Kutty, J. Chen, L. M. Wang, and R. C. Ewing, Ion-irradiation-induced amorphization of $La_2Zr_2O_7$ pyrochlore, Phys. Rev. B 66 (2002) 054108

[6] K. E. Sickafus, L. Minervini, R. W. Grimes, J. A. Valdez, M. Ishimaru, F. Li, K. J. McClellan, T. Hartmann, Radiation tolerance of complex oxides, Science 289 (2000) 748-751

[7] K. E. Sickafus, R.W. Grimes, J.A. Valdez, A. Cleave, M. Tang, M. Ishimaru, S.M. Corish, C. R. Stanek and B.P. Uberuaga, Radiation-induced amorphization resistance and radiation tolerance in structurally related oxides, Nature Mater. 6 (2007) 217-223, DOI: https://doi.org/10.1038/nmat1842

[8] A. A. Bukaemskiy, V. L. Vinograd, P. M. Kowalski, Acta Materialia (2020) Subm.

[9] A. Bogicevic, C. Wolverton, G. Crosbie, and E. Stechel, Defect ordering in aliovalently doped cubic zirconia from first principles, Phys. Rev. B 64 (2001) 014106

[10] A. Bogicevic, and C. Wolverton, Nature and strength of defect interactions in cubic stabilized zirconia, Phys. Rev. B 67 (2003) 024106

[11] J.M. Solomon, J. Shamblin, M. Lang, A. Navrotsky, and M. Asta, Chemical ordering in substituted fluorite oxides: a computational investigation of $Ho_2Zr_2O_7$ and $RE_2Th_2O_7$ (RE=Ho, Y, Gd, Nd, La) Scientific Reports 6 (2016) 38772

[12] A. Predith, G. Ceder, C. Wolverton, K. Persson, T. Mueller, Ab initio prediction of ordered ground-state structures in $ZrO_2$-$Y_2O_3$, Phys. Rev. B 77 (2008) 144104

[13] C. Jiang, C.R. Stanek, K.E. Sickafus, and B.P. Uberuaga, First-principles prediction of disordering tendencies in pyrochlore oxides, Phys. Rev. B 79 (2009) 104203, DOI: https://doi.org/10.1103/PhysRevB.79.104203

[14] S. V. Ushakov, A. Navrotsky, J.A. Tangeman, K.B. Helean, Energetics of defect fluorite and pyrochlore phases in lanthanum and gadolinium hafnates, J. Am. Ceram. Soc. 90 (2007) 1171-1176

[15] M.P. Saradhi, S.V. Ushakov, A. Navrotsky, Fluorite-pyrochlore transformation in $Eu_2Zr_2O_7$ – direct calorimetric measurement of phase transition, formation and surface enthalpies, RSC Adv. 2 (2012) 3328-3334, https://doi.org/10.1039/C2RA00727D

[16] J. Shamblin, M. Feygenson, J. Neuefeind, C. L. Tracy, F. Zhang, S. Finkeldei, D. Bosbach, H. Zhou, R. C. Ewing, and M. Lang, Probing disorder in isometric pyrochlore and related complex oxides, Nature Materials 15 (2016) 507-511

[17] J. Shamblin, C. L. Tracy, R. I. Palomares, E. C. O'Quinn, R. C. Ewing, J. Neuefeind, M. Feygenson, J. Behrens, Ch. Trautmann, M. Lang, Similar local order in disordered fluorite and aperiodic pyrochlore structures, Acta Materialia 144 (2018) 60-67

[18] S. Finkeldei, Ph. Kegler, P.M. Kowalski, C. Schreinemachers, F. Brandt, A.A. Bukaemskiy, V.L. Vinograd, G. Beridze, A. Shelyug, A. Navrotsky, and D. Bosbach, Composition dependent order-disorder transition in $Nd_xZr_{1-x}O_{2-0.5x}$ pyrochlores: A combined structural, calorimetric and ab initio modeling study, Acta Materialia 125 (2017) 166-176

[19] T. A. Lee, A. Navrotsky, I. Molodetsky, Enthalpy of formation of cubic yttria-stabilized zirconia, J. Mater. Res. 18 (2003) 908-918

[20] A. Navrotsky, L. Benoist, H. Lefebvre, Direct calorimetric measurement of enthalpies of phase transitions at 2000°–2400°C in yttria and zirconia, J. Am. Ceram. Soc. 88 (2005) 2942-2944

[21] R. Kikuchi, A theory of cooperative phenomena, Physical Review 81 (1951) 988-1003

[22] A. Finel, The cluster variation method and some applications. In Statics and Dynamics of Alloy Phase Transformations, Edited by P.E.A. Turchi and A. Gonis. Plenum Press, New York, 1994

[23] M.C. Warren, M.T. Dove, E.R. Myers, Monte Carlo methods for the study of cation ordering in minerals, Mineralogical Magazine, 65 (2001) 221-248

[24] D.M. Kerrick, L.S. Darken, Statistical thermodynamic models for ideal oxide and silicate solid solutions, with application to plagioclase, Geochim. Cosmochim. Acta, 39 (1975) 1431-1442

[25] P. Simoncic and A. Navrotsky, Systematics of phase transition and mixing energetics in rare earth, yttrium, and scandium stabilized zirconia and hafnia J. Am. Ceram. Soc. 90 (2007) 2143-2150

[26] A. Navrotsky, Thermodynamics of solid electrolytes and related oxide ceramics based on the fluorite structure, J. Mater. Chem. 20 (2010) 10577-10587

[27] A. Navrotsky, S. Ushakov Thermodynamics of Oxide Systems Relevant to Alternative Gate Dielectrics in A. A. Demkov and A. Navrotsky eds. Materials Fundamentals of Gate Dielectrics 2005, Chapter 3, page 73

[28] P.S. Maram, S.V. Ushakov, R.J.K. Weber, Ch.J. Benmore, and Navrotsky, Probing disorder in pyrochlore oxides using in situ synchrotron diffraction from levitated solids–A thermodynamic perspective Scientific Reports, 8 (2018) 10658, DOI: https://doi.org/10.1038/s41598-018-28877-x

[29] C. Wang. Experimental and computational phase studies of $ZrO_2$-based systems for thermal barrier coatings. PhD Thesis, Stuttgart, 2006

[30] K. Shinozaki, H.R. Sun, K. Uematsu, N. Mizutani, and M. Kato, Sintering of $Sm_2O_3$-$ZrO_2$ Solid Solution, Nippon Kagaku Kaishi 9 (1981) 1454-1461, https://doi.org/10.1246/nikkashi.1981.1454

[31] W. K. Chang, A. A. Wang, and Y. H. Lee, Oxygen-induced structural change of zirconia by adding rare earth oxides with solid state method, J. Alloy Comp. 249 (1997) 251-255, https://doi.org/10.1016/S0925-8388(96)02739-9

[32] Y. Tabira, R. L. Withers, Structure and Crystal Chemistry as a Function of Composition across the Wide Range Nonstoichiometric $(1-\varepsilon)ZrO_2 \cdot \varepsilon SmO_{1.5}$, $0.38<\varepsilon<0.55$, Oxide Pyrochlore System, J. Solid State Chem. 148 (1999) 205-214, https://doi.org/10.1006/jssc.1999.8433

[33] T. van Dijk, K. J. de Vries and A. J. Burggraaf, Electrical Conductivity of Fluorite and Pyrochlore $Ln_x,Zr_{1-x},O_{2-x/2}$ (Ln = Gd, Nd) Solid Solutions, Phys. Stat. Sol. (a) 58 (1980) 115-125

[34] T. Uehara, K. Koto, F. Kanamaru, and H. Horiuchi, Stability and antiphase domain structure of the pyrochlore solid solution in the $ZrO_2$-$Gd_2O_3$ system, Solid State Ionics 23 (1987) 137-143

[35] V.I. Strakhov, J.V. Klucharov, G.G. Sergeev, Interaction of $ZrO_2$ and $Nd_2O_3$ during isothermal treatment (Vzaimodejstvie $ZrO_2$ in $Nd_2O_3$ v uslovijah izotermocheskoj obrabotki, in Russian), Zh. Prikl. Khim. 49 (1973) 2083-2085

[36] J. Wang, A Nakamura, M. Takeda, Structural properties of the fluorite- and pyrochlore-type compounds in the $Gd_2O_3$–$ZrO_2$ system $x$$GdO_{1.5}$–(1-$x$)$ZrO_2$ with $0.18 \leq x \leq 0.62$, Solid State Ionics 164 (2003) 185-191

[37] M. Perez, Y. Jorba, Zirconia-Rare Earth Oxide system, Ann. Chim. 7 (1962) 479

[38] K. Kawata, H. Maekawa, T. Nemoto, T. Yamamura, Local structure analysis of YSZ by Y-89 MAS-NMR, Solid State Ionics 177 (2006) 1687-1690

[39] D. Steele, B.E. Fender, Structure of cubic $ZrO_2$-$YO_{1.5}$ solid solutions by neutron-scattering, J. Phys. C: Solid State Phys. 7 (1974) 1-11

[40] A.I. Ioffe, D.S. Ruthman, and S.V. Karpachov. On the nature of the conductivity maximum in zirconia-based solid electrolytes, Electrochim. Acta 23 (1978) 141-142

[41] W. Baukel, and R. Sheidegger, "Lattice Constants of the Cubic Solid Solution $Zr0_2$-$Y_2O_3$, Ber. Dtsch. Keram. Soc. 45 (1968) 610-616

[42] V.S. Stubican, R.C. Hink, and S.P. Ray, Phase-equilibria and ordering in system $ZrO_2$-$Y_2O_3$, J. Am. Ceram. Soc. 61 (1978) 17-21

[43] M.R. Thornber, D.J.M. Bevan, and E. Summerville, Mixed oxides of the type $MO_2$(fluorite)-$M_2O_3$. V. Phase studies in the systems $ZrO_2$-$M_2O_3$ (M = Sc, Yb, Er, Dy), J. Solid State Chem. 1 (1970) 545-553

[44] Ondik, H. M. & McMurdie, H. F. (eds) Phase Diagrams for Zirconium and Zirconia Systems (The American Ceramic Society, Westerville, 1998

[45] O. Fabrichnaya, M.J. Kriegel, D. Pavlyuchkov, J. Seidel, A. Dzuban, G. Savinykh, G. Schreiber, Heat capacity for the $Eu_2Zr_2O_7$ and phase relations in the $ZrO_2$-$Eu_2O_3$ system: Experimental studies and calculations, Thermochimica Acta, 558 (2013) 74-82

[46] Y. Li, and P.M. Kowalski, G. Beridze, A.R. Birnie, S. Finkeldei, and D. Bosbach, Defect formation energies in $A_2B_2O_7$ pyrochlores, Scripta Materialia 107 (2015) 18-21, https://doi.org/10.1016/j.scriptamat.2015.05.010

.